scientific reports

Check for updates

OPEN

# BrightMice: a low-cost do-it-yourself instrument, designed for in vivo fluorescence mouse imaging

Maylis Boitet[1,2,3], Asma Achek[1], Kelian Bouchenaki[4] & Regis Grailhe[1,2,4]✉

**In vivo fluorescent imaging represents a potent means for real-time probe quantification, facilitating insights into disease pathophysiology and therapeutic responses. Nonetheless, accurate signal quantification remains challenging due to inherent factors like light scattering and tissue absorption. Existing imaging systems, though sophisticated, often entail high costs and are typically restricted to well-funded laboratory settings. This study introduces BrightMice, an innovative in vivo fluorescent imaging system that harnesses 3D printing and consumer-grade digital cameras. Tailored for various fluorophores such as EYFP and E2-crimson, the system showcases both adaptability and effectiveness in detecting in vivo fluorescent signals in several reporter mouse strains. Comparative analyses against commercial instruments confirm BrightMice's sensitivity and underscore its potential to democratize in vivo fluorescence imaging. By providing a cost-effective and accessible solution, BrightMice stands to benefit diverse research environments.**

In vivo fluorescent imaging leverages the unique properties of fluorescent molecules that emit photons upon excitation at specific wavelengths. This powerful technique facilitates real-time quantification of probes, shedding light on the pathophysiology and therapeutic responses of various diseases in living animals[1]. However, challenges persist in accurately quantifying fluorescent signals emitted by tissues in vivo, owing to factors such as light scattering, autofluorescence, and absorptive properties inherent to biological tissues[2]. To address these challenges, the development of far-red and near-infrared probes, including E2-crimson, iRFP713, and iRFP720, has proven instrumental in enhancing the detection of fluorescent signals deep within tissues[3,4].

Despite the widespread use of fluorescent imaging in preclinical studies, there has been limited innovation in imaging systems over the past decade to improve signal and probe quantification. Commonly used in vivo fluorescent imaging instruments typically comprise a dark chamber, a light-emitting source, a set of emission filters, and a camera for signal detection[1]. These planar fluorescence imaging scanners utilize epi-illumination, initially achieved with a white halogen lamp. The required wavelength is carefully selected by passing the light through narrow band-pass excitation filters. Systems from the IVIS series (Revvity, formerly Perkin Elmer) still use this illumination method[5]. With advancements in technology, other light sources, such as LEDs, are now commonly used for epi-illumination in more modern imaging systems due to their greater stability, efficiency, and ability to provide more precise control over the excitation wavelength[6]. This approach is exemplified by the Ami HT system (Spectral Instruments Imaging), which further refines the excitation wavelength by employing an additional layer of narrow band-pass excitation filters.

Recent advancements have primarily focused on increasing throughput by imaging multiple animals simultaneously or integrating anatomical information through combinations with X-ray, CT scans[7], or MRI[8]. This can be achieved through multimodal imaging using two independent systems: one for optical imaging and the other for acquiring anatomical data. This approach requires the use of imaging cassettes compatible between the instruments and requires co-registration of the images. An alternative method involves using fully integrated dual-modality preclinical imaging equipment, which can acquire both optical and X-ray images. Examples of such systems include the Ami HTX and Lago X from Spectral Instruments Imaging as well as the IVIS SpectrumCT from Revvity, which provides 3D optical and CT scan data. However, these sophisticated instruments are prohibitively expensive and are thus confined to research laboratories with substantial budgets.

An alternative approach, in vivo fluorescence tomography, has been developed to ascertain the 3D localization of fluorescent probes[9]. This method reconstructs a 3D fluorescent image of the animal using a

[1]Technology Development Platform, Institut Pasteur Korea, 16, Daewangpangyo-ro 712beon-gil, Bundang-gu, Seongnam-si 13488, Republic of Korea. [2]Division of Bio-Medical Science & Technology, Korea University of Science and Technology, 217 Gajeong-ro Yuseong-gu, Daejeon, Republic of Korea. [3]Core Technology Platforms, New York University Abu Dhabi, P.O. Box 129188, Abu Dhabi, United Arab Emirates. [4]Smart-MD, Institut Pasteur Korea, Seongnam, Republic of Korea. ✉email: regis@smart-mds.com

structured illumination source and acquiring a series of 2D images through light-based transillumination across the entire region of interest. However, three-dimensional (3D) reconstruction remains challenging and is limited to a few specialized systems, as it requires precise modeling of the light path through tissue and calibration of the instrument for each fluorophore based on its optical properties. In this context, the IVIS Spectrum allows for the redirection of the excitation light path from epi-excitation to trans-illumination. This approach minimizes auto-fluorescence background noise and allows deeper penetration of the excitation light, thereby enhancing imaging capabilities and enabling the visualization and quantification of deeper structures within the animal. Nevertheless, the state-of-the-art systems for in vivo fluorescence tomography remain the FMT series including the FMT2500 (Revvity, formerly Perkin Elmer), specifically designed for tomography. These systems are equipped with up to four different lasers emitting in the far-red or near-infrared spectrum, optimizing their transillumination capabilities. While promising in improving depth quantification, a study by Boitet et al.[10] did not show a significant improvement over the widely used epi-fluorescence imaging technique.

Harnessing the accessibility of Light-Emitting Diodes (LEDs), optical filters, and digital cameras, several cost-effective imaging technologies have successfully visualized bacteria and eukaryotic cells expressing fluorescent proteins[11,12]. Strikingly, the application of such approaches to in vivo fluorescence imaging remains underexplored. This study introduces a novel, customizable, and low-cost in vivo fluorescent imaging system named BrightMice, capitalizing on two widely available technologies: 3D printing and consumer-grade digital cameras. The BrightMice system utilizes a modified Sony Alpha mirrorless camera, optimized for detecting the far-red fluorophore E2-crimson[13]. In this study, we utilized the Thy1-EYFP and GFAP- E2crimson reporter mouse strains to demonstrate the capabilities of the BrightMice system for rapid phenotyping of transgenic fluorescent mouse strains. This system effectively detects and quantifies EYFP signals in adult albino mice, as well as far-red fluorescent signals across various developmental stages, from pups to adults, in mice with either albino or agouti fur colors. We further validated our prototype by comparing its signal-to-noise ratios with those of two commercial systems: the FMT2500 from Perkin Elmer and the Ami HT from Spectral Instruments Imaging.

## Results

### Hardware tailored to in vivo fluorescence imaging of EYFP or E2-crimson

For our study, we optimized the BrightMice imaging system for precise excitation and detection of two distinct fluorophores: EYFP (excitation peak at 513 nm, emission peak at 527 nm) and the far-red fluorescent protein E2-crimson (excitation peak at 611 nm, emission peak at 646 nm). To avoid direct detection of the light source by the camera, we strategically ensured a gap of at least 60 nm between the excitation and emission wavelengths. For EYFP, which has a narrow Stokes shift of 14 nm, we used a 470 nm LED excitation source paired with a 466/20 nm narrow bandpass excitation filter (Fig. 1a), resulting in 10% excitation efficiency. Emission was captured using a 525/50 nm bandpass filter, achieving a detection efficiency of 59% (Fig. 1b). For imaging E2-crimson, we used a 590 nm excitation LED, enabling 80% excitation of the fluorophore (Fig. 1c). The selective detection of E2-crimson was improved using two long-pass filters, LP670 nm and LP690 nm, with efficiencies of 38.3% and 24.6% respectively (Fig. 1d). Details of the EYFP and E2-crimson fluorescence detection modules are compiled in Supplementary Table 1. The modular design of BrightMice (Fig. 1e-f) allows for customization to accommodate a wide range of fluorophores, with selectable LEDs and emission filters.

BrightMice consists of multiple 3D printed parts such as the dark chamber of dimension of 180 × 180 × 1250 mm, the door, the roof, the LEDs rack, the mouse movable rack (Supplementary Fig. 1). This one is equipped with a color camera (APS-C Sony A6000) modified full spectrum to accommodate the far-red fluorescence emission of E2-Crimson (Supplementary Fig. 2), a macro lens (FE 50 mn, F1.8) and a polylactic acid (PLA) based 3D printing structure (Fig. 1e). The assembly of all parts is straightforward as described in the Supplementary Fig. 3.

The BrightMice imaging process involves two consecutive acquisitions: first, a reflection image is obtained at a 1/4000 s exposure time without emission filters, to obtain a topographic image of the animal. Second, a fluorescence image is acquired at a 1/30 s exposure time with the emission filters positioned in front of the camera lens, as depicted in Fig. 1e. A summary of camera and imaging parameters can be found in Fig. 1f. This process ensures that only the specific wavelengths of light emitted by the target fluorescent protein, whether E2-crimson or YFP, are selectively captured. It is noteworthy that this operation last less than 10 s, enough for the animals to remain motionless throughout the pre-anesthetized phase.

### BrightMice hardware validation for rapid phenotyping of Thy1-EYFP transgenic mouse strain

In our initial application, we assessed the capability of BrightMice for rapid phenotyping of fluorescent reporter albino mice, which are better suited for fluorescence imaging compared to agouti mice. We selected the widely used Thy1-EYFP mouse strain due to its well-documented high expression levels of EYFP protein in both motor and sensory neurons throughout the brain, with particularly intense fluorescence observed late during the development in adult mice[14]. To begin, we fine-tuned imaging parameters, specifically the excitation and emission channels, for EYFP fluorescence using fixed adult brains from wild-type (WT), Thy1-EYFP, and GFAP-E2crimson mice. The BrightMice system, set up with a 470 nm LED coupled with a BP525/50 nm emission filter, showed specific fluorescence detection for the Thy1-EYFP brain (Supplementary Fig. 4a). Analysis of plot profiles from these brains revealed a noticeable increase in pixel intensity within the green channel of Thy1-EYFP brains compared to the wild-type, and GFAP-E2crimson specimens. Further enhancement of EYFP signal detection was achieved by using a BP466/20 nm excitation filter with the LED arrays. With these optimized settings, the same Thy1-EYFP brain exhibited significantly enhanced green fluorescence (Fig. 2a). Additionally, plot profiles indicated selective expression of EYFP in the cortex but not the cerebellum, consistent with previously reported expression patterns in this reporter strain[15], and further validated through fluorescence microscopy of brain sections (Fig. 2b).

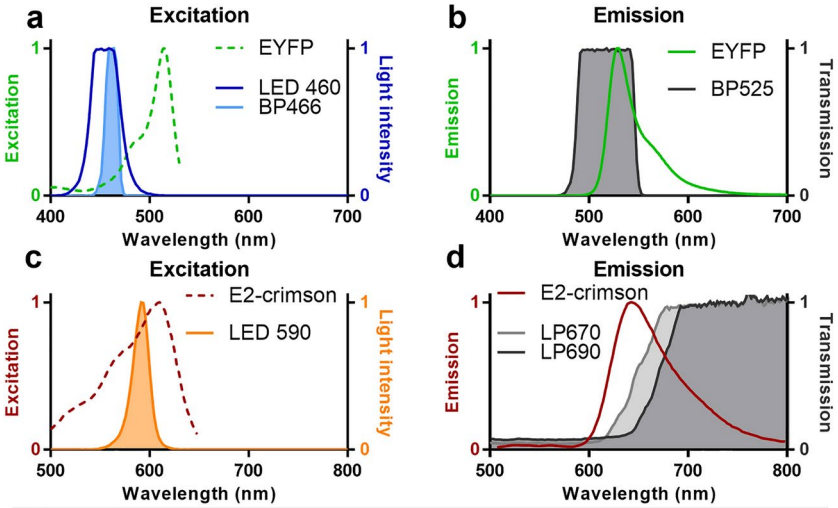


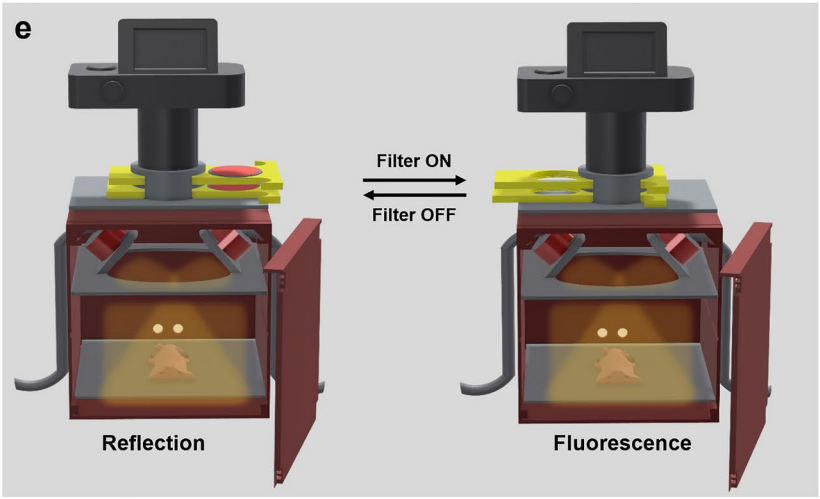


| f | Reflection image | Fluorescence image |
|---|---|---|
| Focus mode | Manual | Manual |
| Aperture | 2.8 | 2.8 |
| ISO | 800 | 800 |
| White balance (K) | 2500 | 2500 |
| Exposure (s) | 1/4000 | 1/30 |
| Filters | No | Yes |
| RGB channel | Green | Red (E2-crimson)<br>Green/Blue (EYFP) |

**Fig. 1**. An in vivo far-red epi-fluorescence imager, named BrightMice, specifically designed for the detection of fluorescent probes. (**a**) Excitation spectrum of the fluorescent EYFP protein obtained from fpbase.org (green dashed line) together with the spectral light intensity of 470 nm LED arrays (depicted in light blue) and the light transmission spectra of the BP466nm bandpass excitation filters (depicted in dark blue). (**b**) Emission spectrum of the fluorescent EYFP protein obtained from fpbase.org (green) together with the light transmission spectra of the bandpass emission filter BP525nm (black). (**c**) Excitation spectrum of the far-red fluorescent E2-crimson protein obtained from fpbase.org (red dashed line) together with the spectral light intensity of 590 nm LED arrays. (**d**) Emission spectrum of the far-red fluorescent E2-crimson protein obtained from fpbase.org (red) together with the light transmission spectra of the RapidEdge long-pass emission filters LP670nm and LP690nm (grey and black). (**e**) Schematic representation of BrightMice operation steps. Two successive images are taken with the full-spectrum-modified APS-C camera. The animal is placed on the mouse rack with its head carefully positioned within the head holder. The 590 nm or 470 nm LED arrays are turned on and the filter rails are placed at the no-filter position. First, a reflection image is acquired using a 1/4000 s exposure time. Then, the emission filters are placed in front of the camera lens before acquiring a fluorescence image at 1/30 s exposure time. (**f**) Summary of BrightMice camera setting for reflection and fluorescence image acquisitions.

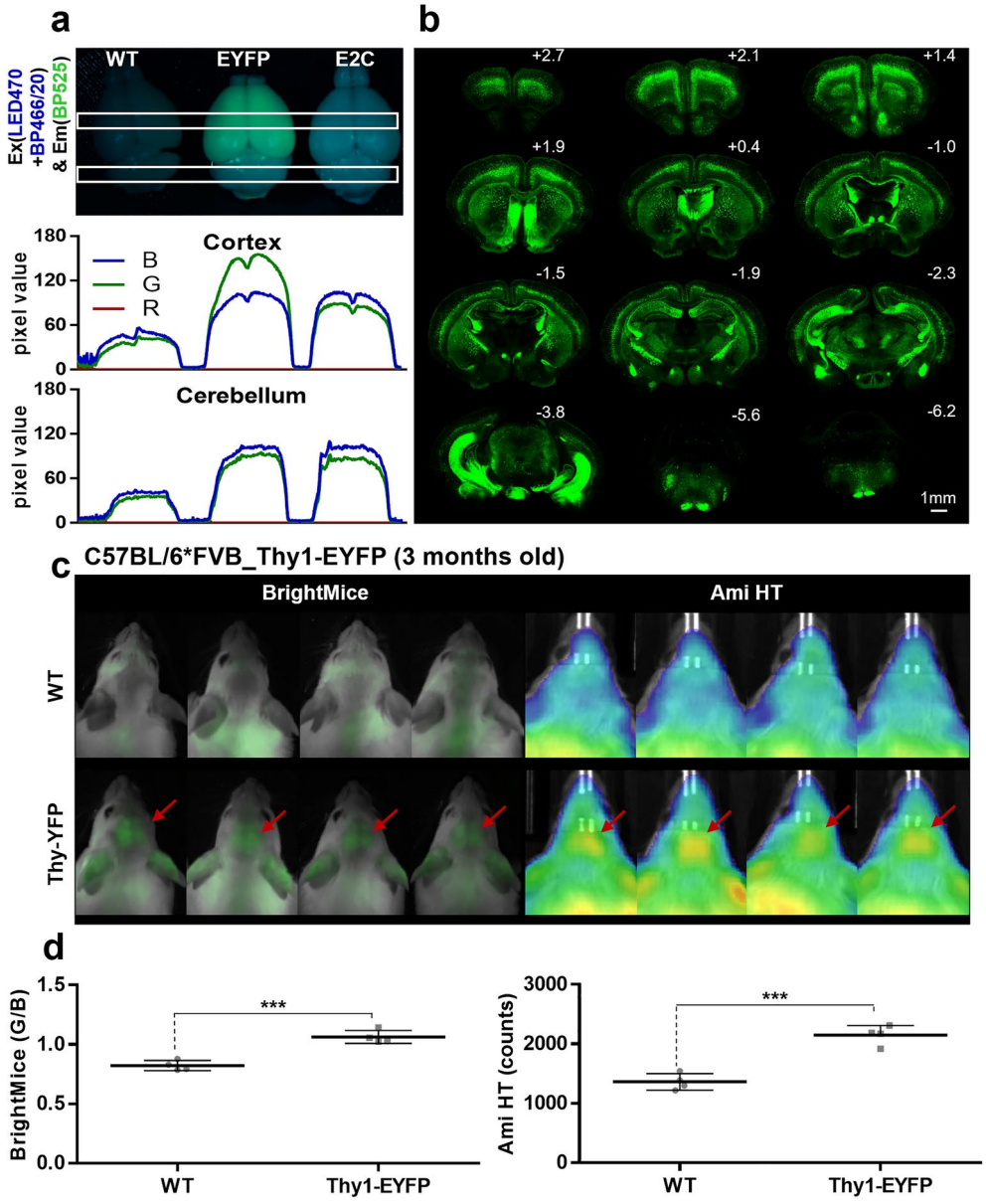


**Fig. 2**. Comparison of BrightMice detection sensitivity for EYFP fluorescent signals with Ami HT. (**a**) Ex vivo fluorescence imaging of wild-type, Thy1-EYFP, and GFAP-E2crimson fixed brains using 470 nm LED arrays with bandpass excitation filters (BP466nm) and a bandpass emission filter (BP525nm) for EYFP detection. Plot profiles of the fluorescence intensity in the cortical and cerebellar regions (white rectangle) were measured for each RGB channel. (**b**) A rostral-to-caudal series of coronal brain slices (40 µm) from a Thy1-EYFP mouse arranged visualized using fluorescent microscopy (Operetta, PerkinElmer) confirming the heterogeneous distribution of EYFP–positive cells across the brain tissues (green labeling). Approximate Bregma coordinates (mm) are indicated at the top of each histological slide. (**c**) In vivo fluorescence imaging of wild-type (n = 4) and Thy1-EYFP (n = 4) mice using BrightMice (overlay of Re and G) and Ami HT from Spectral Instruments Imaging (false color). Red arrows highlight the detection of EYFP signals in the brain area. (**d**) Quantification of the fluorescent signal revealed a significantly higher fluorescence in Thy1-EYFP mice (n = 4) compared to wild-type mice (n = 4) when using the BrightMice and Ami HT systems. Data are presented as a scatter dot plot with the mean ± SD. *p*-values were calculated using unpaired Student's t-tests. ***$p < 0.001$. WT: wild-type; EYFP: Thy1-EYFP; E2C: GFAP-E2crimson; B: blue fluorescence channel; G: green fluorescence channel; R: red fluorescence channel.

Next, BrightMice fluorescence imaging was employed in living adult WT and Thy1-EYFP mice. Fluorescence signals were detectable through the skull and skin in Thy1-EYFP mice, appearing as a greenish signal on the animal's head and confirmed through plot profile analysis (Supplementary Fig. 4b). Adult WT (n = 4) and Thy1-EYFP (n = 4) mice were then sequentially imaged using both BrightMice and Ami HT imager (Fig. 2c). Fluorescent signals were quantified by calculating the ratio of signal intensity detected in the green channel

relative to the blue channel (G/B) using the relative spectral sensitivity of the full spectrum color APS-C camera sensor. Nonspecific fluorescence signals measured in four adult WT mice were quantified at 0.82 ± 0.04 with BrightMice and 1363 ± 138.2 counts with Ami HT. In contrast, fluorescence signals in Thy1-EYFP mice were significantly higher, measured at 1.06 ± 0.05 with BrightMice and 2147 ± 163 counts with Ami HT, respectively (Fig. 2d). Altogether, these results confirm the reliability and suitability of BrightMice for detecting EYFP probes in both ex vivo and in vivo tissues, paving the way for rapid phenotyping of Thy1-EYFP transgenic adult albino colonies.

## BrightMice hardware validation using GFAP-E2crimson transgenic mouse strain

We previously introduced the GFAP-E2crimson transgenic mice, engineered for astrogenesis and astrogliosis quantification in pups and adult respectively. To optimize imaging parameters for the E2-crimson protein, fixed adult brains from WT, Thy1-EYFP, and GFAP-E2crimson mice were examined using BrightMice with two LED excitation sources, coupled with a combination of two long-pass emission filters, LP670 nm and LP690 nm. This setup showed an even distribution of the fluorescence signal across the brain (Supplementary Fig. 5a). Plot profiles derived from these images indicated that the optimal signal dynamics were achieved using an excitation LED emitting at 590 nm, compared to the LED emitting at 630 nm (Supplementary Fig. 5b). Microscopy imaging of GFAP-E2crimson brain sections confirmed the expression of the E2-crimson fluorescent protein across all brain regions, as shown by histological analysis (Supplementary Fig. 5c).

Taking advantage of this reporter mouse model, we were particularly interested in the possibility of phenotyping our transgenic colonies as early as in pups less than 4 days old, which show optimal light penetration and fluorescent signal detection due to the absence of hair and the thinness of the skull (Supplementary Fig. 6). The pups were gently placed in a small black beaker before being inserted into the BrightMice system for fluorescence imaging. As shown in Supplementary Video 1, the E2-crimson signal was also easily detectable in freely moving transgenic GFAP-E2crimson pups, confirming the capacity of BrightMice as a potential tool for early and rapid phenotyping of litters from mouse colonies.

Next, adult WT FVB (n = 4), hemizygous GFAP-E2crimson (n = 12), and homozygous GFAP-E2crimson mice (n = 8) were sequentially imaged using BrightMice and two commercial in vivo fluorescent imager FMT2500 and Ami HT systems (Fig. 3a). Nonspecific fluorescent signals in adult FVB were measured at 22.69 ± 0.66 FLU (Fluorescent Relative Unit), 88.72 ± 6.34 count/energy, and 101.8 ± 21.25 counts using BrightMice, FMT2500, and Ami HT, respectively (Fig. 3b). E2-crimson signals emitted in hemizygous and homozygous GFAP-E2crimson mice were measured at 46.34 ± 2.96 FLU and 70.97 ± 4.98 FLU using BrightMice. For the FMT2500 system, quantification of E2-crimson signals was established at 112.8 ± 4.61 count/energy and 159.8 ± 7.97 count/energy, respectively, in hemizygous and homozygous GFAP-E2crimson mice. Similarly, quantification of E2-crimson signals using Ami HT was measured at 291.2 ± 15.65 counts and 545.4 ± 52.04 counts, respectively, in hemizygous and homozygous GFAP-E2crimson mice. Beyond demonstrating BrightMice's ability to differentiate significant expression levels between all phenotypes, strong correlations were found between fluorescent data acquired with the BrightMice system and values obtained using FMT2500 ($R^2 = 0.9599$) and Ami HT ($R^2 = 0.928$), demonstrating BrightMice's accurate performance in in vivo fluorescence imaging, as presented in Fig. 3c.

To assess the sensitivity of each instrument for detecting E2-crimson, we compared the fluorescent signals emitted from GFAP-E2crimson transgenic mice and wild-type mice. Signal ratios (SR) between transgenic and non-transgenic mice were determined from the heads of both hemizygous and homozygous GFAP-E2crimson mice (Fig. 3d-e). Despite efforts to mitigate background endogenous nonspecific fluorescence by shaving the animals' heads before in vivo fluorescence imaging, background signals remained relatively elevated. Consequently, the total signal includes both the specific E2-crimson signal and non-specific fluorescence, which can be attributed to nonspecific fluorescence and light reflection. The specific E2-crimson fluorescent signal can be accurately quantified through a secondary calculation, achieved by applying a threshold to eliminate the nonspecific fluorescence inherent in wild-type animals. The signal ratios obtained with the BrightMice system were 2.04 ± 0.13 for hemizygous and 3.13 ± 0.22 for homozygous GFAP-E2crimson mice, falling between the SR values obtained with the FMT2500 and Ami HT systems (Fig. 3d-e). Specifically, SR values for the FMT2500 were 1.27 ± 0.05 for hemizygous and 1.8 ± 0.09 for homozygous GFAP-E2crimson mice, while the Ami HT system yielded SR values of 2.86 ± 0.15 for hemizygous and 5.36 ± 0.51 for homozygous GFAP-E2crimson mice. Consequently, the full-spectrum APS-C digital camera used in BrightMice was found to be extremely sensitive and capable of quantifying far-red fluorescent signals compared to the dedicated CCD camera mounted on the FMT2500 and Ami HT equipment. To assess Brightmice's capability to track dynamic changes over time, we conducted a time series of in vivo fluorescence imaging on homozygous GFAP-E2crimson pups (n = 3) from 2 to 30 days post-natal, using the three instruments (Fig. 4). Post-natal quantification of E2-crimson signals showed a rapid increase from day 2 to day 7, followed by a decrease until day 30 of age, associated with skull thickening and fur appearance, as reported by Boitet et al.[10]. Comparison between the instruments demonstrated similar E2-crimson expression dynamics, reflecting the astrogenesis occurring during the pups' brain development.

Since many available transgenic animals have dark fur pigmentation (black coat color), we next challenged our systems' respective sensitivity in quantifying E2-crimson through tissues with higher absorptive properties. In vivo fluorescence imaging of wild-type agouti (n = 5) and agouti GFAP-E2crimson (n = 5) mice—obtained from breeding between C57BL/6 and albinos FVB GFAP-E2crimson—was performed using BrightMice, FMT2500, and Ami HT systems as presented in Supplementary Fig. 7a. Nonspecific fluorescence signals from agouti wild-type mice were measured at 7.04 ± 1.42 FLU, 36.62 ± 0.38 counts/energy, and 83.09 ± 7.32 counts, respectively, using BrightMice, FMT2500, and Ami HT (Supplementary Fig. 7b). Similarly, E2-crimson signals from homozygous GFAP-E2crimson mice with agouti color coat were measured at 19.82 ± 5.10 FLU with BrightMice, 43.67 ± 3.86 counts/energy with FMT2500, and 169.5 ± 14.94 counts with Ami HT (Supplementary Fig. 7b).

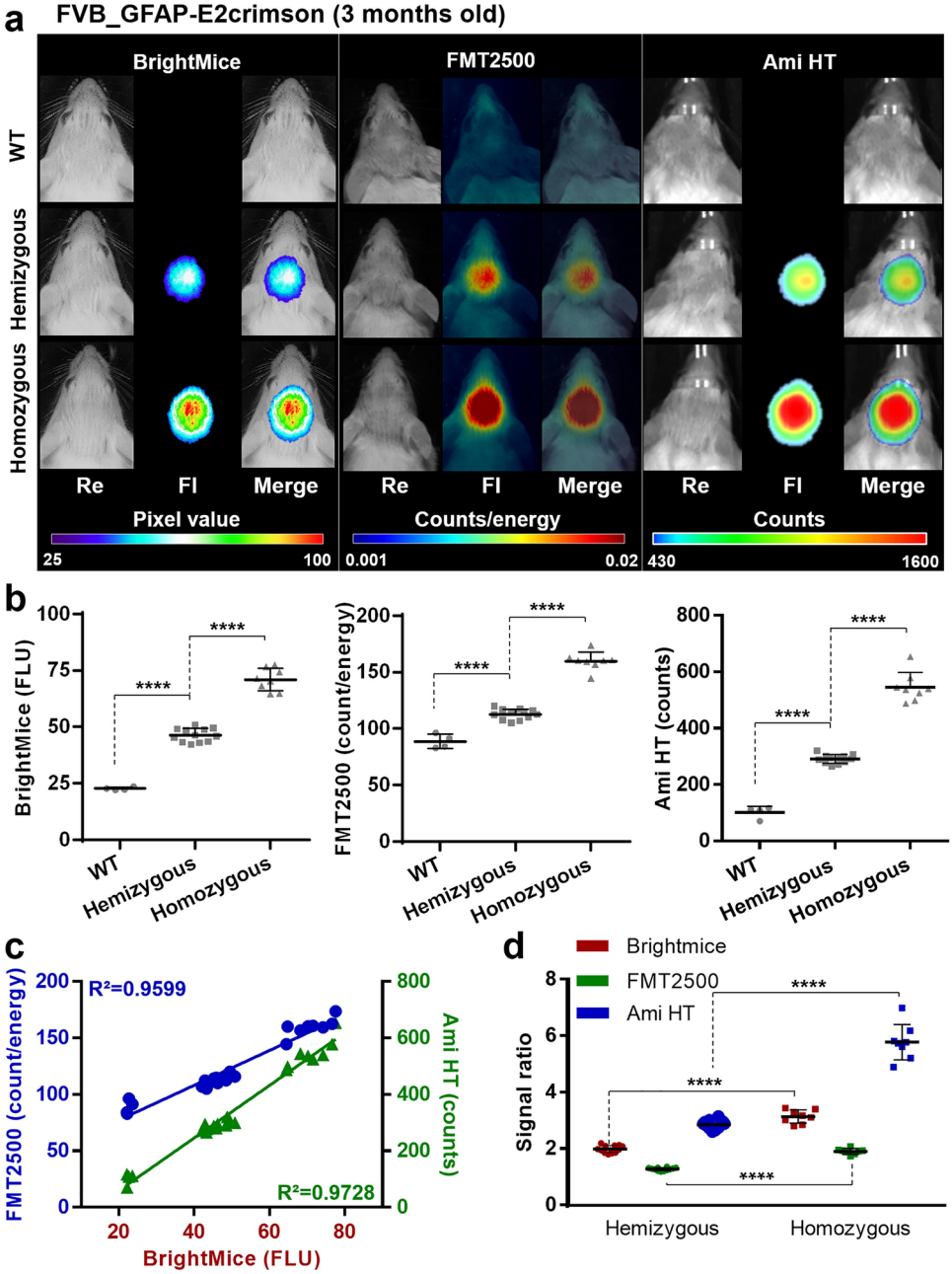


e

| | SR Hemizygous | SR Homozygous |
|---|---|---|
| BrightMice | 2.04±0.13 | 3.13±0.22 |
| FMT2500 | 1.27±0.05 | 1.80±0.09 |
| Ami HT | 2.86±0.15 | 5.36±0.51 |

As presented in Supplementary Fig. 7c-d, signal/noise ratios were established at 2.81 ± 0.72 for BrightMice, 1.19 ± 0.11 for FMT2500, and 2.04 ± 0.18 for Ami HT, confirming BrightMice's ability to discriminate specific E2-crimson signals. This capability can be easily employed for the rapid phenotyping of transgenic reporter mice with agouti fur color.

## Discussion

In vivo fluorescence imaging holds significant importance in biomedical research as it allows for the direct observation and quantification of biological events in small animals. This is achieved through the detection of signals emitted by exogenous fluorescent probes and dyes, as well as the visualization of fluorescently labeled cells or transgenic reporter animals. The rapidly growing number of fluorescent probes in the far-red and near-infrared window is steadily expanding the applications and complexity (multiplexing) of in vivo fluorescence

◀**Fig. 3**. Comparison of BrightMice detection sensitivity for far-red fluorescent signals with two commercial in vivo imaging systems: FMT2500 and Ami HT. (**a**) In vivo fluorescence imaging of wild-type, hemizygous and homozygous GFAP-E2crimson mice using BrightMice, FMT2500 (Perkin Elmer) and Ami HT (Spectral Instruments Imaging). (**b**) Quantification of fluorescent signal in wild-type mice (n = 4), hemizygous (n = 12) and homozygous (n = 8) GFAP-E2crimson mice, using BrightMice, FMT2500, and Ami HT systems. In wild-type mice, only the nonspecific auto-fluorescence signal is detected. Data are presented as a scatter dot plot with the mean ± SD. *p*-values were calculated using unpaired Student's t-tests. ****$p < 0.0001$. (**c**) Comparison of far-red fluorescent signals obtained from wild-type, hemizygous and homozygous GFAP-E2crimson mice for BrightMice and FMT2500 (blue labels) and for BrightMice and Ami HT (green labels). (**d**) Signal ratios of hemizygous and homozygous GFAP-E2crimson mice quantified using BrightMice, FMT2500 and Ami HT systems. Background noise was estimated by averaging the auto-fluorescence background value of 4 wild-type mice. Data are presented as a scatter dot plot with the mean ± SD. *p*-values were calculated using unpaired Student's t-tests. ****$p < 0.0001$. (**e**). Average signal to background noise ratios of hemizygous and homozygous GFAP-E2crimson mice obtained using BrightMice, FMT2500 and Ami HT. WT: wild-type; Hemizygous: hemizygous GFAP-E2crimson; Homozygous: homozygous GFAP-E2crimson; Re: reflection image; Fl: fluorescence image; FLU: Fluorescent Relative Unit; SR: signal ratio.

imaging[7] that is now used in preclinical studies[16], oncology[17], neurology[18] or immunology[19]. Most in vivo optical imaging systems are today able to perform both fluorescence and bioluminescence imaging when equipped with a highly sensitive cooled CCD camera. In contrast to fluorescence imaging, in vivo bioluminescence imaging offers an exceptionally high signal-to-noise ratio[20]. However, it necessitates longer exposure times (several minutes) due to the inherently weak bioluminescent signals. Additionally, the technique requires systemic administration of a luciferase substrate[21,22], which has complex pharmacokinetics[23] that must be carefully managed. This requirement can potentially limit the feasibility of performing multiple time-point imaging.

This study presents BrightMice, a low-cost full-spectrum digital camera-based in vivo fluorescence imaging system designed to quantify far-red fluorescent signals. Our practical solution provides a viable option for implementing in vivo fluorescence imaging in biomedical research laboratories that face limitations in terms of space or financial resources. For just 1% of the cost of high-end alternatives like the Spectral Ami HT and FMT 2500, BrightMice stands out as a remarkably cost-effective solution (Supplementary Tables 1–3). BrightMice takes advantage of 3D printing technology for manufacturing, the reduced cost of light sources such as LEDs and broad spectral sensitivity of CMOS sensors from consumable cameras[24]. In recent decades, the consumer market's fierce competition has led to significant advancements in CMOS sensor technology, now reaching the performance of CCD sensors commonly employed in scientific equipment such as microscopes, gel imagers, and in vivo imagers. CMOS detectors offer enhanced dynamic range, resolution, and sensitivity, thereby unlocking new possibilities for low-light applications such as bioluminescence imaging[25] and astronomical imaging[26]. To date, there have been no documented reports on the quantification of in vivo far-red fluorescent signals using CMOS sensors. This is primarily due to the design of digital cameras, which are optimized to capture photons within the visible window below 650 nm, rendering them less suitable for deep tissue in vivo fluorescence imaging. In order to overcome this limitation and harness the sensor sensitivity for far-red fluorescent signals, we have extended the detection range well beyond 650 nm by removing its embedded mirrorless filter.

During the development of the BrightMice system, we meticulously selected the light source and emission filters to precisely match the fluorescence properties of EYFP and E2-crimson fluorescent proteins, while minimizing nonspecific signals. Irrespective of the fluorescent protein used, our findings revealed that the excitation light must be carefully selected and tested both spectrometrically and experimentally. For example, the LED 590 demonstrated superior results compared to the LED 630 for E2-crimson. Additionally, the LED 470 signal was significantly improved with the use of an additional excitation filter (BP466/20), resulting in an increased EYFP fluorescence signal relative to background noise. This phenomenon was attributed to the emission filters inadequately blocking the reflected excitation wavelengths from reaching the detector (Supplementary Figs. 4a-5a). Our improved outcomes were achieved by ensuring a strict separation of excitation and emission wavelengths facilitated by two key adjustments: (1) employing an excitation LED with a relatively narrow emission wavelength shorter than the excitation peak of the fluorescent protein and (2) utilizing relatively broad pass emission filters (such as a long-pass filter or 50 nm band-pass filter), whenever feasible, longer than the emission peak of the fluorophore of interest to capture maximal emitted light. In specific cases, we deliberately maintained the widest separation (60–80 nm) between the median excitation source and the cut-on emission wavelength. Consequently, BrightMice proves to be well-suited for the quantification of in vivo visible and far-red fluorescent signals, a validation confirmed through the use of both Thy1-EYFP and GFAP-E2crimson reporter mouse strain. When compared to other in vivo imaging equipment such as the FMT2500 and Ami HT instrumentations, BrightMice exhibited a pronounced selectivity for detecting the EYFP and E2-crimson fluorescent signals.

Despite the considerable challenges posed by the high scattering and absorption of light within the visible range[27,28], BrightMice demonstrated sufficient specificity to detect EYFP fluorescent signals from albino Thy1-EYFP mice. Similar to the Ami HT, it offers a rapid and non-invasive phenotyping solution, providing insight into the transgene expression levels. This can effectively substitute conventional mouse genotyping techniques, which typically require tissue biopsy and do not provide information regarding transgene expression levels. Such capability could be expanded to enable rapid phenotyping of any albinos or hairless fluorescent reporter mouse strains meeting specific criteria, such as exhibiting a bright fluorescent protein within the visible spectrum[29], displaying robust transgene expression, and harboring this expression primarily in relatively shallow tissue

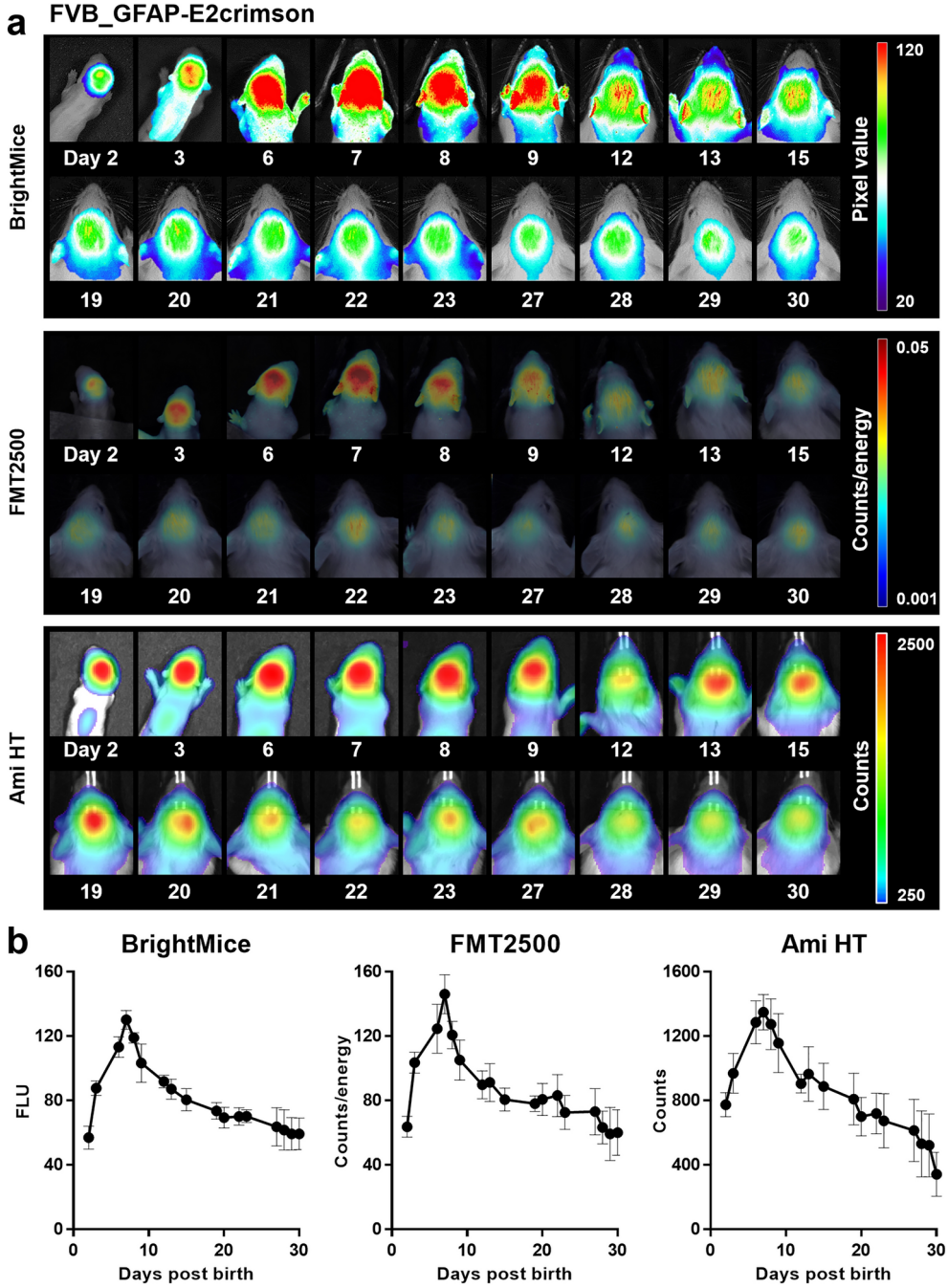


**Fig. 4**. In vivo quantification of post-natal E2-crimson signals over a one-month period using three in vivo epi-fluorescent imagers: BrightMice, FMT2500, and Ami HT. (**a**) Representative in vivo fluorescence imaging of homozygous GFAP-E2crimson pups using BrightMice, FMT2500 and Ami HT systems for a period of 30 days. (**b**) In vivo quantification of E2-crimson fluorescent signals in homozygous GFAP-E2crimson pups (n = 3) from 2 to 30 days of age displayed a similar time course when using the BrightMice, FMT2500, and Ami HT systems. Data are presented as mean ± SD. FLU: Fluorescent Relative Unit.

layers. Moreover, BrightMice outperformed both commercial systems in quantifying E2-crimson intensity in agouti GFAP-E2crimson mice. We attribute this success to the careful attention we put into selecting the optimal excitation and emission wavelengths for each fluorophore, rather than developing equipment with a broad array of wavelengths for general purposes.

In our study, it is essential to acknowledge the limitations of the commercial systems employed. Firstly, it is imperative to recognize that the FMT2500 has undergone extensive development and optimization specifically for excelling in 3D fluorescence tomography. Consequently, the FMT2500 is equipped with a restricted number of channels within the far-red region, and its camera parameters (exposure time, f-stop, binning, etc.) are fixed in the software. While the laser-based transilluminator of the FMT2500 facilitates precise 3D reconstruction,

enabling independent quantification of probe quantity irrespective of its depth, it is important to note that this system is not explicitly tailored for in vivo epi-fluorescence imaging. This limitation is attributed to the narrow wavelength gap of 25 nm between the 635 nm excitation LEDs and the BP660/20 nm emission filter on the FMT2500, resulting in unintended detection of excitation light that leaks through to reach the sensor.

On the other hand, the Ami HT is equipped with excitation (465 nm and 605 nm) and emission (BP530/20 nm and BP660/20 nm) channels optimized for the detection of the EYFP and E2-crimson proteins respectively, ensuring excellent fluorescence detection. Additionally, the Ami HT provides more versatility for users in selecting imaging parameters such as exposure time, f-stop, binning, and field of view. Notably, the minimum exposure time on the Ami HT hardware is 0.5 s. Despite the -90 °C absolute cooled CCD camera, a 1-s exposure time is required to reach the minimum detection level of EYFP and E2-crimson probe in our transgenic mouse models. This exposure time is approximately 30–33 times longer than those required for the FMT2500 and BrightMice, respectively. This discrepancy may be attributed to the detector on the Ami HT, which has a lower quantum efficiency than the one installed on the FMT2500.

In our earlier studies, we successfully demonstrated the utility of CMOS digital cameras in quantifying faint bioluminescent signals expressed in both eukaryotic and prokaryotic systems. This was accomplished using a microplate imager known as Biolum' RGB[25]. Therefore, it would be intriguing to explore the potential of BrightMice in conducting in vivo bioluminescence imaging utilizing highly luminescent probes such as NanoLuc or AkaLuc luciferases in future investigations.

While initially validated with the Thy1-EYFP and GFAP-E2crimson reporter mouse, the BrightMice system has the potential for broader applications in various in vivo fluorescent imaging scenarios within the visible or far-red spectrum. This versatility stems from its mirrorless CMOS sensor, which maintains sensitivity to photons emitted at wavelengths up to 1050 nm (data not shown). In such cases, it is crucial to carefully select and optimize the excitation LED and emission filters based on the specific fluorophore of interest. Additionally, during image analysis, it is important to consider the relative transmissivity of the RGB channels within the emission wavelength range of the fluorophore to ensure accurate selection of the channel with the highest sensitivity. This allows for optimal performance and adaptability of the BrightMice system in a wide range of imaging applications spanning from the visible to the far-red wavelength range.

Another notable aspect worth mentioning is the compact size of the BrightMice system, which provides an additional advantage. In comparison to the FMT2500 and Ami HT instrumentations, the BrightMice system is significantly smaller, being approximately 19 and 43 times more compact, respectively (Supplementary Fig. 8). This compactness enables convenient placement of the BrightMice system within a biosafety cabinet, which is particularly beneficial for studying infectious diseases in ABSL2-4 facilities or laboratories with limited space. The ability to operate within such confined environments further enhances the practicality and versatility of the BrightMice system for various research settings.

## Materials & methods

### 3D model design and printing

BrightMice represents a cost-effective in vivo epi-fluorescence imaging system, featuring a mirrorless Sony Alpha A6000 camera coupled with a Sony 50 mm (F2.8) Macro lens. The Sony A6000 boasts an APS-C (23.5 × 15.6 mm) sensor with a 24-megapixel image resolution and RGB capability, encompassing red, green, and blue channels. Given the inherent limitation of digital cameras to visible light sensitivity (approximately 400 to 650 nm), the camera underwent modification to attain full-spectrum capability. This modification involved replacing the hot mirror in front of the sensor with a full-spectrum glass filter. Consequently, our camera can capture visible light, UV, and, crucially, detect far-red wavelengths (350–800 nm), as illustrated in Supplementary Fig. 1.

The BrightMice system comprises distinct 3D-printed components, including a box, roof, LED rack, mouse rack, door, two filter rails, and magnet holders. Eight round magnets (5-mm diameter, 3-mm thickness) secure the door firmly in place. The design of BrightMice was executed using computer-assisted design (CAD) software (Autodesk 123D, USA) and implemented through 3D printing with an Ultimaker 3 printer (Ultimaker, Netherlands) using polylactic acid (PLA) filament. Printing parameters were set at a layer height of 0.2 mm, infill density of 20%, and a printing temperature of 205 °C. To reduce light reflection from the LED on the plastic components, we applied two layers of super matte water-based acrylic paint (Black 2.0, Stuart Semple) to all internal elements of the box. This was followed by a coating of Belton clear matte transparent paint (Molotov, Germany), ensuring both waterproofing and facilitating easy cleaning with water-based detergent. All STL files necessary to construct BrightMice are included in the supplementary material.

### BrightMice assembly

The steps for assembling and using BrightMice are depicted in Supplementary Figs. 2–3. In essence, the design of the dark chamber took into consideration the maximum printing capacity of an average 3D printer, aiming for cost-effective printing while minimizing the need for 3D printing support. Consequently, the resulting box has dimensions of approximately 180 × 180 × 250 mm and consists of two parts: the roof and the box. After the printing process, the initial step involves permanently attaching the roof to the box using polycyanoacrylate (super glue). To ensure the complete opacity of the box for imaging, magnets can be permanently affixed to both the door and the box. The mouse rack is positioned approximately 1 cm above the box floor, while the LED rack is situated about 10 cm from the box ceiling. Based on the specific fluorophore being studied, the appropriate LED arrays—and excitation filters (20 mm of diameter), if necessary—are inserted into the holder that comes with the rack. The power cable is then routed through the lateral holes designed into the rack. Similarly, emission filters are installed in their designated racks. Emission filters with a diameter of 50 mm are positioned on the filter rail rails to selectively detect fluorescence signals with the digital camera.

For this study, the following LED arrays were utilized: one emitting at 470 nm (LIU470A, Thorlabs, USA, 4.0 mW/cm$^2$ at 100 mm, 253mW), another at 590 nm (LIU590A, Thorlabs, USA, 1.4 mW/cm$^2$ at 100 mm, 109mW) and a third at 630 nm (LIU630A, Thorlabs, USA, 2.4 mW/cm$^2$ at 100 mm, 208mW). These LED arrays were employed for the selective excitation of EYFP or E2-crimson. A BP525/50 nm bandpass filter (Omega Optical Inc., USA) as well as RapidEdge longpass LP670nm and LP690nm filters (Omega Optical Inc., USA) were employed for the selective emission of the two fluorophores. Additionally, bandpass excitation filters (466/20 nm) were utilized to refine the intensity and wavelength of excitation light for EYFP. The light intensity spectra of the different LEDs and the light transmission spectra of the excitation and emission filters used in this study were measured using a Lumini TWO spectrometer (Myspectral Lumini Ltd., USA). A breakdown of the hardware costs for BrightMice can be found in Supplementary Table 1.

## Animal husbandry

All mice in this study were housed in standard individually ventilated cages, subjected to a 12-h light–dark cycle, and had unrestricted access to food and water. The GFAP-E2crimson mouse strain, developed in our facility with an FVB background, was employed in this investigation. This strain, recently characterized for its ability to report in vivo astrogliosis, has been documented in a recent publication[10]. To increase genetic diversity, GFAP-E2crimson mice with an FVB background were crossbred with C57BL/6 mice for two generations, resulting in progeny that were wild-type, hemizygous, and homozygous for the GFAP-E2crimson gene on an agouti background. Similarly, Thy1-EYFP (B6.Cg-Tg(Thy1-YFP)HJrs/J) mice with a C57BL/6 background[14,30] (strain #003,782, The Jackson Laboratory) were bred with FVB mice for two generations to obtain albinos Thy1-EYFP mice.

The animal protocols governing this study received approval from the Institutional Animal Care and Use Committee of Institut Pasteur Korea, with the following approved protocol numbers: IPK-22004 and IPK-22012. The study design and all procedures followed the ARRIVE Guidelines.

## BrightMice camera settings, in vivo fluorescence imaging and image analysis using Fiji

To enhance the consistency of experimental conditions, the full-spectrum camera was configured in manual mode, capturing images in both JPEG and RAW formats onto a memory card. However, for the purposes of this study, only the JPEG files were subjected to processing. This decision aligns with our previous findings, as discussed by Boitet et al.[25], where no significant dynamic range improvement was observed with the utilization of RAW files.

The camera settings for the BrightMice system were standardized, with a white balance of 2500 K, ISO set to 800, and aperture at F2.8 (Fig. 1f). Initially, image focus was established using autofocus on a dedicated target at the experiment's outset, followed by a switch to manual focus mode.

To ensure the immobility of the mice during imaging, they were anesthetized within an induction chamber, employing an isoflurane/oxygen mixture. Careful positioning on the animal rack preceded the reinsertion of the rack into BrightMice. The door is closed before initiating imaging.

Image analysis was performed using Fiji, an open-access software, to quantify fluorescent signals within a predefined Region of Interest (ROI) located on the animal's head. The JPEG images were first separated into three channels (red, green, and blue). The analysis primarily focused on the red channel to capture the E2-crimson signal, leveraging its enhanced sensitivity to far-red wavelengths. Conversely, EYFP signals were analyzed using the distinctive spectral selectivity of the green and blue channels, which are more suitable for detecting the wavelengths emitted by YFP. Quantification was performed by calculating the ratio of fluorescent signal intensity detected in the green channel relative to that in the blue channel. The ROI was carefully designed to encompass the entire brain region of the animal and saved using the ROI Manager plugin, ensuring consistency in quantifying fluorescent signals across different experiments. For adult mice, the same ROI was consistently applied for fluorescence signal quantification, while a smaller ROI was used for pups to accommodate their size. Additionally, the ROI was precisely positioned using anatomical landmarks—the corner of the eye and the midpoint of the ear—to ensure consistent coverage of the entire brain region (Supplementary Fig. 9). This precise positioning was performed prior to determining the average fluorescence intensity of the signal. To calculate signal ratios between transgenic and wild-type animals, the baseline autofluorescence background was first obtained by averaging the non-specific signals detected from control animals. The fluorescence signals from transgenic animals were then divided by this baseline. The results were defined as signal ratios. Additionally, plot profiles of the fixed brains were obtained after channel splitting, utilizing the Plot Profile macro.

## In vivo fluorescence imaging using FMT2500 and Ami HT systems

In vivo E2-crimson fluorescence imaging was conducted using the FMT2500 system, setting the lowest feasible excitation wavelength at 635 nm (LED) with an exposure time fixed at 0.03 s, and employing a 650–670 nm emission bandpass filter (BP660/20 nm). Before imaging, the animals were anesthetized in an induction chamber with an isoflurane/oxygen mixture to ensure immobilization, and then positioned in the imaging cassette of the FMT2500. Similarly, the far-red fluorescent signals of the same animals were captured using the Ami HT system, with an excitation wavelength of 605/20 nm, an exposure time of 1 s, and emission wavelengths ranging from 640 to 660 nm (BP650/20 nm). Furthermore, in vivo quantification of EYFP signals was performed exclusively with the Ami HT, as the FMT 2500 is only equipped for imaging and quantifying far-red fluorescent signals. The Ami HT was configured with an excitation wavelength of 465/20 nm, an exposure time of 1 s, and emission wavelengths from 520 to 540 nm (BP530/20 nm). Details of the excitation and emission channels for all three imaging systems are summarized in Supplementary Table 2.

Following image acquisition, the TrueQuant software (Perkin Elmer, USA) was used for quantifying fluorescent signals obtained with the FMT 2500. Images from the Ami HT system were analyzed using AURA

imaging software (Spectral Instruments Imaging, USA). In both instances, the ROI covered the entire brain region and was meticulously centered on the animal's head to ensure data reproducibility. Similarly, for each system, the same ROI size was used consistently for all adult animals across experiments. A smaller ROI was designed for pups to accommodate their size. Signal ratios between transgenic and control animals were calculated in the same manner as described for BrightMice. Additional hardware specifications are comprehensively compared in Supplementary Table 3.

### Comparative study of BrightMice, FMT2500, Ami HT systems relative sensitivity

Before conducting fluorescence imaging, each animal underwent systematic head-shaving to enhance the fluorescence signal and minimize background noise from nonspecific fluorescence. Subsequent in vivo fluorescence imaging was conducted sequentially, starting with the FMT2500, followed by the Ami HT and then the BrightMice systems.

Initially, adult mice from various fur colors and transgene expressions were used for in vivo far-red fluorescence imaging. This cohort included albinos wild-type mice (n = 4), hemizygous GFAP-E2crimson mice (n = 12), and homozygous GFAP-E2crimson mice (n = 8). Similarly, mice with an agouti coat color either wild-type (n = 5) and homozygous GFAP-E2crimson (n = 5), were imaged with three different instruments the FMT2500, Ami HT, and BrightMice systems, using their respective channels specifically tailored for E2-crimson detection. Additionally, albinos homozygous GFAP-E2crimson mice (n = 3) underwent fluorescence imaging to monitor astrogenesis from 2 days post-birth to 1 month of age, using the same imaging instruments.

Similarly, albinos wild-type mice (n = 4) and Thy1-EYFP reporter mice (n = 4) were imaged using the Ami HT and BrightMice systems which were specifically adjusted for YFP detection.

### Postmortem histology

Briefly, GFAP-E2crimson and Thy1-EYFP mice underwent successive transcardiac perfusion with phosphate-buffered saline (PBS) followed by paraformaldehyde 4% (PFA) until the body hardened. The brains were then harvested, fixed in PFA, and cryopreserved in sucrose. The tissues were then sectioned using a cryostat (Leica CM 1510S, Germany) into 40 µm thick coronal slices. These brain slices were mounted on slides and imaged using a 10 × magnification objective lens on an Operetta system (Perkin Elmer, USA). The imaging wavelengths were set at 460–490 nm for excitation and 500–550 nm for emission to visualize EYFP, and 600–630 nm for excitation with 650–760 nm for emission to detect E2-crimson. Approximate Bregma coordinates, based on Paxinos and Franklin's reference atlas[31], are indicated on the figures.

### Statistical analysis

The data presented in the graphs are expressed as the mean ± standard deviation (SD). Statistical analysis was conducted using nonparametric unpaired Student's t-tests.

## Data availability

Source data of graphs plotted in every Figures and Supplementary Figures are available as source data files. All STL files required to construct BrightMice are provided as supplementary material.

Received: 26 June 2024; Accepted: 13 September 2024
Published online: 30 September 2024

## References

1. Leblond, F., Davis, S. C., Valdés, P. A. & Pogue, B. W. 'Pre-clinical whole-body fluorescence imaging: Review of instruments, methods and applications. *J. Photochem. Photobiol. B* **98**(1), 77–94 (2010).
2. Lifante, J., Shen, Y., Ximendes, E., Martín Rodríguez, E. & Ortgies, D. H. The role of tissue fluorescence in in vivo optical bioimaging. *J. Appl. Phys.* **10**(1063/5), 0021854 (2020).
3. Luker, K. E. et al. Comparative study reveals better far-red fluorescent protein for whole body imaging. *Sci. Rep.* **5**, 1–9. https://doi.org/10.1038/srep10332 (2015).
4. Isomura, M., Yamada, K., Noguchi, K. & Nishizono, A. Near-infrared fluorescent protein iRFP720 is optimal for in vivo fluorescence imaging of rabies virus infection. *J. Gen. Virol.* **98**(11), 2689–2698. https://doi.org/10.1099/jgv.0.000950 (2017).
5. Cool, S. K., Breyne, K., Meyer, E., De Smedt, S. C. & Sanders, N. N. Comparison of in vivo optical systems for bioluminescence and fluorescence imaging. *J. Fluoresc.* **23**(5), 909–920. https://doi.org/10.1007/s10895-013-1215-9 (2013).
6. Leblond, F., Davis, S. C., Valdés, P. A. & Pogue, B. W. Pre-clinical whole-body fluorescence imaging: Review of instruments, methods and applications. *J. Photochem. Photobiol. B* **98**(1), 77–94. https://doi.org/10.1016/j.jphotobiol.2009.11.007 (2010).
7. Refaat, A. et al. In vivo fluorescence imaging: success in preclinical imaging paves the way for clinical applications. *BioMed. Cent.* https://doi.org/10.1186/s12951-022-01648-7 (2022).
8. Zhang, Y., Zhang, B., Liu, F., Luo, J. & Bai, J. In vivo tomographic imaging with fluorescence and MRI using tumor-targeted dual-labeled nanoparticles. *Int. J. Nanomed.* **9**(1), 33–41. https://doi.org/10.2147/IJN.S52492 (2013).
9. Vasquez, K. O., Casavant, C. & Peterson, J. D. Quantitative whole body biodistribution of fluorescent-labeled agents by non-invasive tomographic imaging. *PLoS One* **6**(6), e20594. https://doi.org/10.1371/journal.pone.0020594 (2011).
10. Boitet, M., Eun, H., Lee, T., Kim, J. & Grailhe, R. Non - invasive in vivo brain astrogenesis and astrogliosis quantification using a far - red E2 - crimson transgenic reporter mouse. *Mol. Neurobiol.* https://doi.org/10.1007/s12035-022-02997-y (2022).
11. Nuñez, I. et al. Low cost and open source multi-fluorescence imaging system for teaching and research in biology and bioengineering. *PLoS One* **12**(11), 1–21. https://doi.org/10.1371/journal.pone.0187163 (2017).
12. Hasan, M. M., Alam, M. W., Wahid, K. A., Miah, S. & Lukong, K. E. A low-cost digital microscope with real-time fluorescent imaging capability. *PLoS One*. https://doi.org/10.1371/journal.pone.0167863 (2016).
13. Strack, R. L. et al. A rapidly maturing far-red derivative of DsRed-Express2 for whole-cell labeling. *Biochemistry* **48**(35), 8279–8281. https://doi.org/10.1021/bi900870u (2009).
14. Porrero, C., Rubio-Garrido, P., Avendaño, C. & Clascá, F. Mapping of fluorescent protein-expressing neurons and axon pathways in adult and developing Thy1-eYFP-H transgenic mice. *Brain Res.* **1345**, 59–72. https://doi.org/10.1016/j.brainres.2010.05.061 (2010).

15. Zhang, Z. et al. Multi-scale light-sheet fluorescence microscopy for fast whole brain imaging. *Front. Neuroanat.* https://doi.org/10.3389/fnana.2021.732464 (2021).
16. Kobayashi, H. et al. Multimodal nanoprobes for radionuclide and five-color near-infrared optical lymphatic imaging. *ACS Nano* **1**(4), 258–264. https://doi.org/10.1021/nn700062z (2007).
17. Koyama, Y. et al. In vivo molecular imaging to diagnose and subtype tumors through receptor-targeted optically labeled monoclonal antibodies. *Neoplasia* **9**(12), 1021. https://doi.org/10.1593/NEO.07787 (2007).
18. Yang, M., Luiken, G., Baranov, E. & Hoffman, R. M. Facile whole-body imaging of internal fluorescent tumors in mice with an LED flashlight. *Biotechniques* **39**(2), 170–172. https://doi.org/10.2144/05392BM02 (2005).
19. Leslie, J., Robinson, S. M., Oakley, F. & Luli, S. Non-invasive synchronous monitoring of neutrophil migration using whole body near-infrared fluorescence-based imaging. *Sci. Rep.* https://doi.org/10.1038/s41598-021-81097-8 (2021).
20. Tung, J. K., Berglund, K., Gutekunst, C.-A., Hochgeschwender, U. & Gross, R. E. Bioluminescence imaging in live cells and animals. *Neurophotonics* **3**(02), 1. https://doi.org/10.1117/1.nph.3.2.025001 (2016).
21. Close, D. M., Xu, T., Sayler, G. S. & Ripp, S. In vivo bioluminescent imaging (BLI): Noninvasive visualization and interrogation of biological processes in living animals. *Sensors*. https://doi.org/10.3390/s110100180 (2011).
22. Xu, T. et al. The expanding toolbox of in vivo bioluminescent imaging. *Front. Res. Found.* https://doi.org/10.3389/fonc.2016.00150 (2016).
23. Berger, F., Paulmurugan, R., Bhaumik, S. & Gambhir, S. S. Uptake kinetics and biodistribution of 14C-d-luciferin-a radiolabeled substrate for the firefly luciferase catalyzed bioluminescence reaction: Impact on bioluminescence based reporter gene imaging. *Eur. J. Nucl. Med. Mol. Imaging* **35**(12), 2275–2285. https://doi.org/10.1007/s00259-008-0870-6 (2008).
24. Ravindran, S. How DIY technologies are democratizing science. *Nature* **587**(7834), 509–511. https://doi.org/10.1038/d41586-020-03193-5 (2020).
25. Boitet, M. et al. Biolum' RGB: A low-cost, versatile, and sensitive bioluminescence imaging instrument for a broad range of users. *ACS Sens.* **7**(9), 2556–2566. https://doi.org/10.1021/acssensors.2c00457 (2022).
26. Greffe, T. et al. Characterization of low light performance of a CMOS Sensor for ultraviolet astronomical applications. In *X-Ray, Optical, and Infrared Detectors for Astronomy X*, A. D. Holland and J. Beletic, Eds., SPIE, Aug. 2022, p. 13. https://doi.org/10.1117/12.2629198.
27. Ntziachristos, V., Ripoll, J., Wang, L. V. & Weissleder, R. Looking and listening to light: The evolution of whole-body photonic imaging. *Nat. Biotechnol.* https://doi.org/10.1038/nbt1074 (2005).
28. Jacques, S. L. Erratum: Optical properties of biological tissues: A review. *Phys. Med. Biol.* https://doi.org/10.1088/0031-9155/58/14/5007 (2013).
29. Luker, K. E. et al. Comparative study reveals better far-red fluorescent protein for whole body imaging. *Sci. Rep.* https://doi.org/10.1038/srep10332 (2015).
30. Feng, G. et al. Imaging neuronal subsets in transgenic mice expressing multiple spectral variants of GFP. *Neuron* **28**(1), 41–51. https://doi.org/10.1016/S0896-6273(00)00084-2 (2000).
31. George. Paxinos and K. B. J. Franklin, 'Paxinos and Franklin's The mouse brain in stereotaxic coordinates', 2019.


## Acknowledgements

The authors would like to express their great appreciation to Adrien Mesnard and Sangjun Yoon for their valuable support in designing 3D parts of BrightMice dark chamber.

## Author contributions

M.B. participated in the design of the BrightMice technology, performed the animal experimentation, analyzed data, and drafted the manuscript. A.A. participated in the animal experimentation and revision of manuscript. K.B. designed the BrightMice hardware. RG designed and supervised the study and wrote the manuscript. All authors read and approved the final manuscript.

## Funding

MB was supported by the UST Young Scientist Research Program through the University of Science and Technology [2018-YS-06C]. RG laboratory was supported by the National Research Foundation of Korea (NRF), grant funded by the Korean government [MSIT, project number NRF-2023M3A9G6057281]. The funders had no role in study design, data collection and analysis, decision to publish, or preparation of the manuscript.

## Competing interests

The authors declare that they have no competing interests.

## Additional information

**Supplementary Information** The online version contains supplementary material available at https://doi.org/10.1038/s41598-024-73130-3.

**Correspondence** and requests for materials should be addressed to R.G.